Proceedings of the ASME 2017 Internal Combustion Engine Division Fall Technical Conference
ICEF2017
October 15-18, 2017, Seattle, Washington, USA

ICEF2017-3662

CFD SIMULATIONS OF THE EFFECT OF WATER INJECTION CHARACTERISTICS ON TSCI: A NEW, LOAD-FLEXIBLE, ADVANCED COMBUSTION CONCEPT

Mozhgan Rahimi Boldaji
Department of Mechanical Engineering
Stony Brook University
Stony Brook, New York, USA

Aimilios Sofianopoulos
Department of Mechanical Engineering
Stony Brook University
Stony Brook, New York, USA

Sotirios Mamalis
Department of Mechanical Engineering
Stony Brook University
Stony Brook, New York, USA

Benjamin Lawler
Department of Mechanical Engineering
Stony Brook University
Stony Brook, New York, USA

ABSTRACT

Homogeneous Charge Compression Ignition (HCCI) combustion has the potential for high efficiency with very low levels of NOx and soot emissions. However, HCCI has thus far only been achievable in a laboratory setting due to the following challenges: 1) there is a lack of control over the start and rate of combustion, and 2) there is a very limited and narrow operating range. In the present work, the injection of water directly into the combustion chamber was investigated to solve the aforementioned limitations of HCCI. This new advanced combustion mode is called Thermally Stratified Compression Ignition (TSCI).

A 3-D CFD model was developed using CONVERGE CFD coupled with detailed chemical kinetics to gain a better understanding of the underlying phenomena of the water injection event in a homogeneous, low temperature combustion strategy. The CFD model was first validated against previously collected experimental data. The model was then used to simulate TSCI combustion and the results indicate that injecting water into the combustion chamber decreases the overall unburned gas temperature and increases the level of thermal stratification prior to ignition. The increased thermal stratification results in a decreased rate of combustion, thereby providing control over its rate. The results show that the peak pressure and gross heat release rate decrease by 37.8% and 83.2%, respectively, when 6.7 mg of water were injected per cycle at a pressure of 160 bar. Finally, different spray patterns were simulated to observe their effect on the level of thermal stratification prior to ignition. The results show that symmetric patterns with more nozzle holes were generally more effective at increasing thermal stratification.

INTRODUCTION

Internal combustion (IC) engines play an important role in transportation and stationary power generation. US Government projections for the transportation sector indicate that the IC engine will remain the dominant prime mover for the next several decades [1]. For this reason, it is paramount to achieve both high efficiency and low levels of harmful emissions from IC engines. Low temperature combustion (LTC) is one potential technology that achieves high efficiency with low levels of harmful emissions. Homogeneous Charge Compression Ignition (HCCI) is one example of an LTC mode, which combines the favorable characteristics of both diesel and spark ignition (SI) engines. However, HCCI suffers from a lack of control over the start and rate of combustion, which results in a limited operating range.

In recent years, research has focused on strategies to control the start of ignition and heat release in HCCI. One such strategy that has been investigated is exhaust gas recirculation (EGR) [1-6]. Yao et al. [2-4] indicated that the EGR rate is an important parameter for controlling HCCI combustion. They showed that by adjusting the external, cooled EGR rate, the ignition timing and combustion duration can be regulated to some extent. Yap et al. [5] combined inlet charge boosting with internal, hot EGR in a single cylinder engine to extend its upper load HCCI limit. Cairns and Blaxill proposed employing both internal and external EGR in order to expand the upper load limit [6]. They were able to extend the upper load limit by 20-65% when higher external EGR fractions were considered. Another strategy for controlling heat release in HCCI is Variable Compression Ratio (VCR). Heyvonen et al. [7] combined VCR and inlet air preheating by exhaust heat recovery in an attempt to expand the

operating range in their HCCI engine. However, the application of VCR has been limited since it requires complex hardware and engine designs.

Another strategy aimed at controlling LTC heat release that has been explored in the literature is charge stratification. Charge stratification is a method that creates areas with varying equivalence ratios in the cylinder. Charge stratification can be achieved by direct injection of fuel in the combustion chamber at different timings during compression. Aroonsrisopon et al. [8] used this technique in HCCI in an experimental study on a Cooperative Fuel Research (CFR) engine in order to expand the operating range. They used two injectors; one in the intake system to create an overall homogenous mixture and one in the combustion chamber to control the level of stratification by changing the relative mass injected by each injector and/or the injection timing. Although this strategy expanded the HCCI operating range, it reduced combustion efficiency and increased NO_x, UHC, and CO emissions [9].

Many of the LTC strategies have attempted to use charge stratification to control the heat release process including Premixed Charge Compression Ignition (PCCI) [10-12], Gasoline Compression Ignition (GCI) [13-15], Gasoline Direct Injection Compression Ignition (GDCI) [16], Partial Fuel Stratification (PFS) [17], and even Reactivity Controlled Compression Ignition (RCCI) [18-20]. While these combustion modes have demonstrated success in terms of controllability and expanded operating range, the intentional mixture inhomogeneity has an inherent risk of elevated soot and NOx emissions.

Recently Lawler et al. [21] proposed a new approach, called Thermally Stratified Compression Ignition (TSCI), which introduces a forced thermal stratification in HCCI by using direct injection of water into the combustion chamber. Injecting water directly into the combustion chamber affects the level of thermal stratification, and therefore allows control over the LTC heat release process. The experimental results indicated a gross IMEP range expansion from 2.3-3.6 bar in pure HCCI to 2.3-8.4 bar in TSCI. Additionally, the results showed that by adjusting the amount of injected water, the combustion phasing and burn rate can be varied, providing control over both the start and rate of heat release. In the current work, Computational Fluid Dynamics (CFD) modeling is used to provide insight into the effects of water injection pressure and spray characteristics on TSCI combustion.

Water injection has been previously investigated in diesel engines to reduce NO_x emissions [22-28]. Bedford and Rutland [22] used CFD modeling to study the effect of water injection in a diesel engine and found that the vaporization of water reduced the production of both NO_x and soot emissions at low loads. Hountalas et al. [26] investigated two different technologies of water injection to reduce NO_x emissions in a heavy duty diesel engine: water-fuel emulsions and the injection of water into the intake manifold. They suggested that the water emulsion was more effective at reducing NO_x compared to intake manifold injection; however, it incurred a penalty in soot and brake specific fuel consumption (BSFC). Water injection has also been shown to reduce NO_x emissions in SI engines [29, 30]. Additionally, water injection has been experimentally investigated in advanced combustion concepts such as HCCI and PCCI [31-34]. These studies concluded that water injection can control ignition timing, decelerate the heat release process, and expand the operating range in advanced combustion engines.

In the present work, a 3D CFD model of an HCCI engine is utilized to investigate the underlying phenomena that occur due to water injection. The model is first validated against experimental data from Lawler et al. [21] for both pure HCCI without water injection (WI) and for TSCI with WI. Second, the effect of injection pressure on combustion is investigated. Finally, different spray patterns are simulated to understand their effects on thermal stratification in HCCI.

3D CFD MODEL DEVELOPMENT AND VALIDATION

In this paper, a 3D CFD model was developed using CONVERGE CFD [35] coupled with detailed chemical kinetics. The mechanism presented by Liu et al. [36] was utilized. It was developed for primary reference fuel (PRF) oxidation and consists of 41 species and 124 reactions. The ignition delay of the mechanism developed by Liu et al. [36] was validated against shock tube experiments and the species evolution was validated against jet-stirred reactor and flow reactor experimental data for HCCI-relevant conditions. The mechanism was then validated in an HCCI engine using a 3D CFD model developed in KIVA-3V [37] for PRF73 and PRF70 and its ability to predict HCCI combustion was showcased.

In all of the simulations presented in this paper, a blend of 10% n-heptane and 90% isooctane was selected as the fuel. The simulations were performed of a single cylinder of a production 4-cylinder 2.0L engine manufactured by General Motors (type LNF). This was the same engine that was used in the experimental work of Lawler et al. [21]. The production engine needed some modifications to enable HCCI combustion and conduct the experiments including NVO camshafts and a higher compression ratio piston. For more information on the experimental setup, please refer to [21]. Table 1 summarizes the engine specifications, including the engine speed which is 2000 rpm for all the results presented in this paper.

TABLE 1. ENGINE SPECIFICATIONS

Bore	86 mm
Stroke	86 mm
Connecting rod length	145.5 mm
Compression ratio	12.5:1
Valve timings	IVO -276°, IVC -150°, EVO 148°, EVC 274°
Fuel	PRF90
Engine speed	2000 rpm

The fuel and air were inducted into the combustion chamber through the intake runner and the side-mounted direct injector

was used to inject water directly into the combustion chamber. Initial conditions for the simulations, including the equivalence ratio and combustion chamber pressure, temperature, and EGR fraction were taken from the experimental data, then adjusted slightly during the validation process to achieve good agreement. Additionally, a few of the sub-model constants have been tuned, while most of them were kept at their default values. These adjustments could be due to the uncertainty in the experimental data in determining quantities like the internal residual gas fraction or bulk cylinder temperature and due to uncertainty in the sub-models. Some of the inputs to the CFD simulation are compared to their experimental counterparts in Table 2. Simulations were performed for three consecutive cycles and the results at the end of each cycle were mapped for each mesh cell to initialize the next cycle.

In this work, a Reynolds-Averaged Navier-Stokes (RANS) approximation is used to solve the Navier-Stokes equations coupled with the renormalization group (RNG) k-ε turbulence model [38, 39]. The Kelvin-Helmholtz and Rayleigh-Taylor (KH-RT) [40-42] model is used to solve the breakup of the water spray droplets. For the calculation of drop drag coefficient, the dynamic drop drag model of Liu et al. [43] is used. Collison between spray droplets is simulated through the No Time Counter (NTC) method [44]. In addition, a wall film sub-model is used to model interaction of liquid drops with solid surfaces [35]. This model predicts different outcomes due to drop/wall interaction including wall film depositing, drop rebounding, drop splashing, and film stripping. Finally, for droplet evaporation, the Chiang et al. [45] correlation is used.

The SAGE combustion model [46] is coupled with the multi-zone model of Babajimopoulos et al. [47], which has shown significantly lower computational cost while maintaining accuracy [48]. Law of wall boundary conditions are used for velocity and temperature and the O'Rourke and Amsden [37, 49] law of wall model is used to model the flow field adjacent to the wall. A base orthogonal cut-cell grid of 4 mm is utilized while the mesh size is reduced around the intake and exhaust valves to 0.5 mm, in the entire combustion chamber to 1 mm, and around the injector to 0.25 mm. Additionally, adaptive mesh refinement (AMR) is used to refine the mesh at the regions of the flow field with high sub-grid values of temperature, velocity, and HO_2, OH, CO, and O_2 species mass fraction.

Figure 1 shows a view of the CFD model. The computational domain included three distinct regions: the intake port, exhaust port, and combustion chamber, each of which was initialized separately. The inter-region boundaries (valves and valve seats) were used for flow control between the ports and the combustion chamber.

The CFD model described above was validated against two different conditions: 1) Pure HCCI without water injection, and 2) TSCI with water injection. The operating conditions for these two validation cases are listed in Table 2.

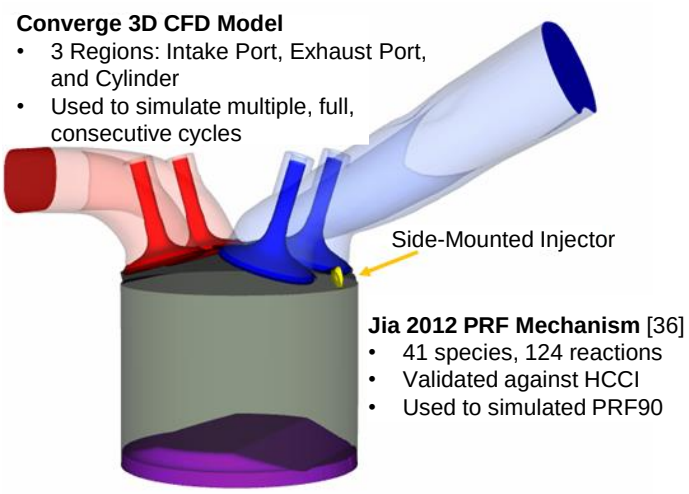

Figure 1. Schematic of the CFD engine geometry

TABLE 2. OPERATING CONDITION OF 2 VALIDATED CASES

	Pure HCCI	TSCI with water injection
Simulation wall temperature	430 K	430 K
Experiment wall temperature	Not Directly Measured	Not Directly Measured
Simulation intake temperature	373 K	388 K
Experiment intake temperature	403 K	433 K
Simulation equivalence ratio	0.74	0.74
Experiment equivalence ratio	0.74	0.74
Simulation residual rate	0.45	0.44
Experiment residual rate	0.41	0.4

Validation of Pure HCCI

A thorough validation of the computational results was performed against the previously collected experimental data in [21]. The comparison between CFD simulation results and experimental data for pure HCCI without water injection (WI) is shown in Figure 2. The engine speed was 2000 rpm and the load was 3.7 bar gross IMEP.

Figure 2 indicates good agreement between the CFD simulation and the experimental results, which provides confidence in the ability of the model to capture pure HCCI combustion.

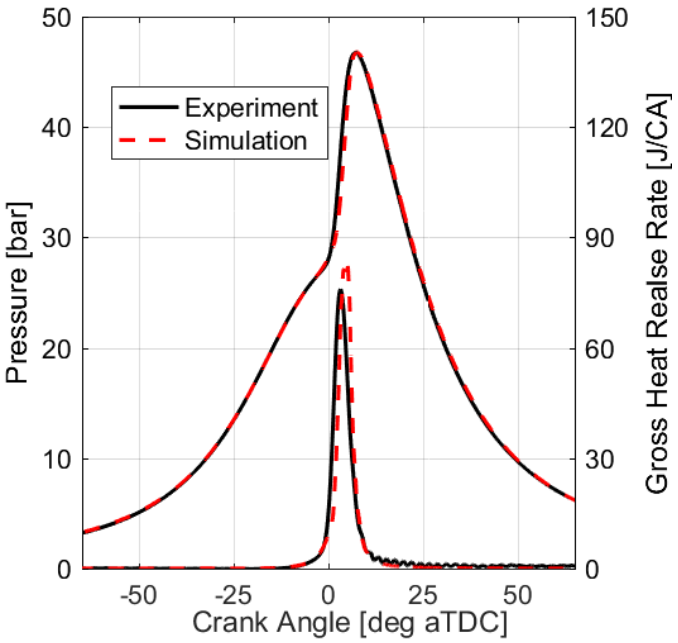

Figure 2. Comparison between the CFD model and experimental results for pure HCCI without water injection

Validation of TSCI with Water Injection

A comparison between CFD and experimental data for TSCI with water injection is plotted in Figure 3. The mass of water injected per cycle was 6.7 mg at a start of injection (SOI) timing of -50° crank angle degrees (CAD) after top dead center (aTDC) and the injection duration was 11.5 CAD. The specifications of the injector are listed in Table 3. The engine speed was 2000 rpm and the load was about 3.7 bar gross IMEP.

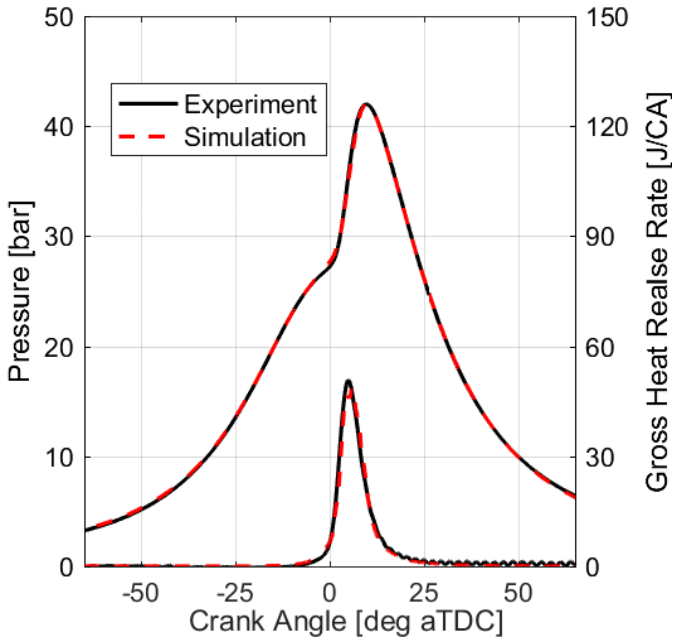

Figure 3. Comparison between the CFD model and experimental results for TSCI with water injection

TABLE 3. INJECTOR SPECIFICATIONS

	Default Values	Range
Number of nozzle holes	6	1-6
Injection spray type	Solid cone spray	
Nozzle diameter	0.2 mm	
Spray cone angle	26°	
Injection duration	11.5 CAD	4-11.5 CAD
SOI	-50° aTDC	
Injected water pressure	19.3 bar	19.3-160 bar
Injected water temperature	295 K	
Mounting type	Side-mounted	

The column of "Default Values" in Table 3 describes the default configuration that was used to collect the experimental data and is therefore used in Figure 3 to validate the CFD model in TSCI. The "Range" column in Table 3 describes the range of each particular parameter that will be explored in this paper. Figure 3 shows very good agreement between the simulation and the experimental results, providing confidence in the ability of the model to accurately capture TSCI. Comparing Figure 2 to Figure 3, the peak pressure and heat release rate are reduced in TSCI. The previous experimental work suggested that this is due to the evaporative cooling effect of the water injection which introduces a forced thermal stratification [21]. Water droplets evaporate and absorb heat from the surrounding mixture, thereby cooling the nearby regions and resulting in increased thermal stratification and lower heat release rates. In this way, TSCI uses water injection to control the start of combustion and the heat release rate in LTC. With this significantly enhanced control, TSCI is able to considerably extend the operating range compared to pure HCCI [21].

RESULTS AND DISCUSSION

Following the validation effort in both pure HCCI and TSCI, simulations were performed to investigate the effects of water injection, including the injection pressure and the spray pattern, on ignition and heat release in TSCI.

Effect of Water Injection Pressure on Combustion

Simulations were performed for pure HCCI without water injection (WI) and TSCI with WI with varying injection pressure to study the effect of water injection pressure on combustion. For all TSCI with WI injection cases, the mass of injected water was kept constant (6.7 mg) while the injection duration was varied to compensate for the changing injection pressure.

Figure 4 indicates that injecting water into the combustion chamber at 19.3 bar retards the combustion phasing by 5.7 CAD (CA50 changes from 0.4° CAD to 6.1° CAD), decreases the peak pressure from 52 bar to 42.1 bar (19.2%), and reduces the maximum heat release rate (HRR) from 132 J/CA to 48.5 J/CA (63.2%). This behavior was attributed to the evaporative cooling effect of the water injection. The water droplets evaporate and absorb energy from the surrounding mixture, which reduces the

in-cylinder temperature. The aforementioned reduction in temperature also results in increased thermal stratification (as will be discussed in more detailed in Figures 5, 6, and 7). This demonstrates how water injection can be used to control both the start and the rate of heat release in LTC.

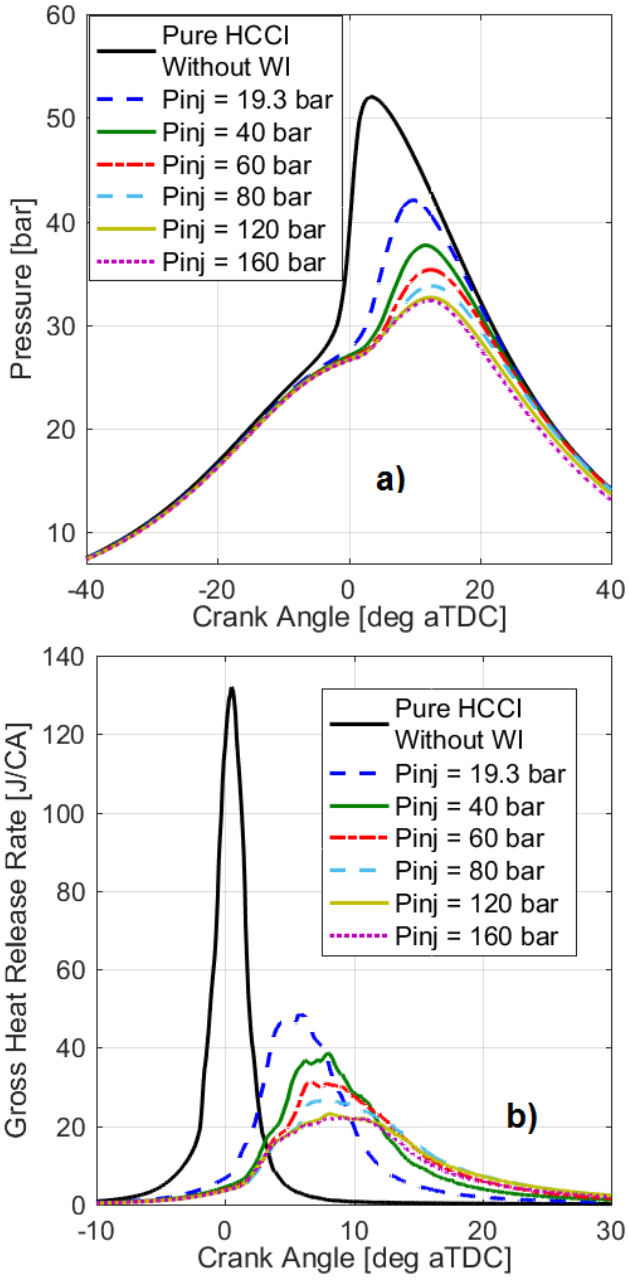

Figure 4. Effect of water injection pressure on a) the cylinder pressure and b) heat release rate

Figure 4 also shows that increasing the pressure of injection results in lower peak cylinder pressure and peak HRR, and also further retards the start of combustion. Increasing the injection pressure amplifies the effects of water injection by further increasing the level of stratification due to better breakup and evaporation of the water droplets, which is in agreement with previously published studies on gasoline sprays indicating that higher injection pressure in a gasoline direct injection (GDI) engine improved the spray breakup process and its evaporation rate [50-52]. The peak HRR reduced by 63.2%, 71%, 76.4%, 79.7%, 82.5%, and 83.2% for injection pressures of 19.3, 40, 60, 80, 120, and 160 bar, respectively, when compared to the pure HCCI case. The peak pressure decreased by 19.2%, 27.5%, 32.5%, 35.1%, 37.2%, and 37.8% compared to pure HCCI.

Figure 5 illustrates the effect of injection pressure on the mass-temperature distribution prior to combustion at -11° CAD after top dead center (aTDC) for the maximum and minimum injection pressures compared against the pure HCCI case. This specific timing, -11° CAD, was chosen because it is before the start of heat release, which would begin to affect the mass-temperature distribution. The mass probability density functions (PDFs) shown in Figure 5 represent the density of mass at a given temperature. The mass PDF is calculated from the CFD results of the temperature and mass in each mesh cell at a specific CAD (in this case -11° CAD). The mass-temperature distributions in Figure 5 are filtered with a weak filter that helps interpret the results. A more thorough discussion of the filtering of the CFD mass-temperature distributions is included in the appendix.

Figure 5 shows that water injection reduces the mass density at high temperatures and distributes that mass over a larger range of lower temperatures. The reduced in-cylinder temperatures, which result from the evaporative cooling of the WI, retards combustion phasing, while the broader mass-temperature distribution reduces the heat release rate. Increasing the pressure of injection decreases the in-cylinder temperatures further and amplifies the effect of WI on the width of the mass-temperature distribution.

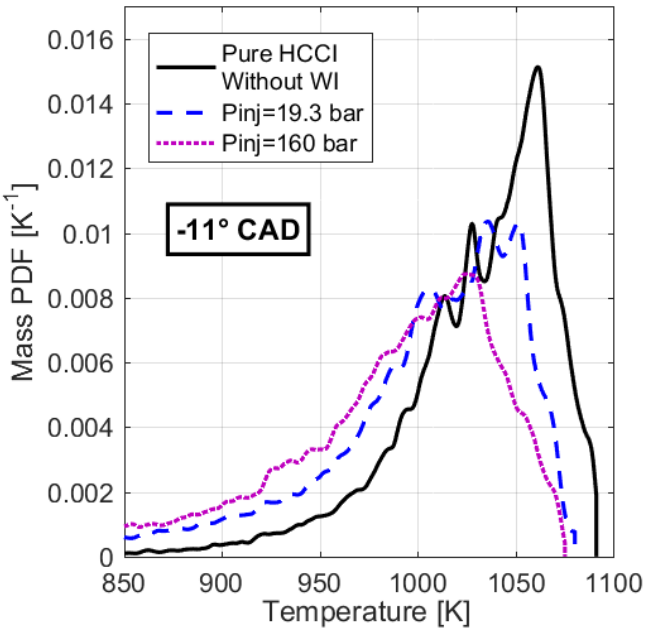

Figure 5. The in-cylinder mass-temperature distribution prior to ignition represented as mass probability density functions (Mass PDFs) versus temperature for different injection pressures

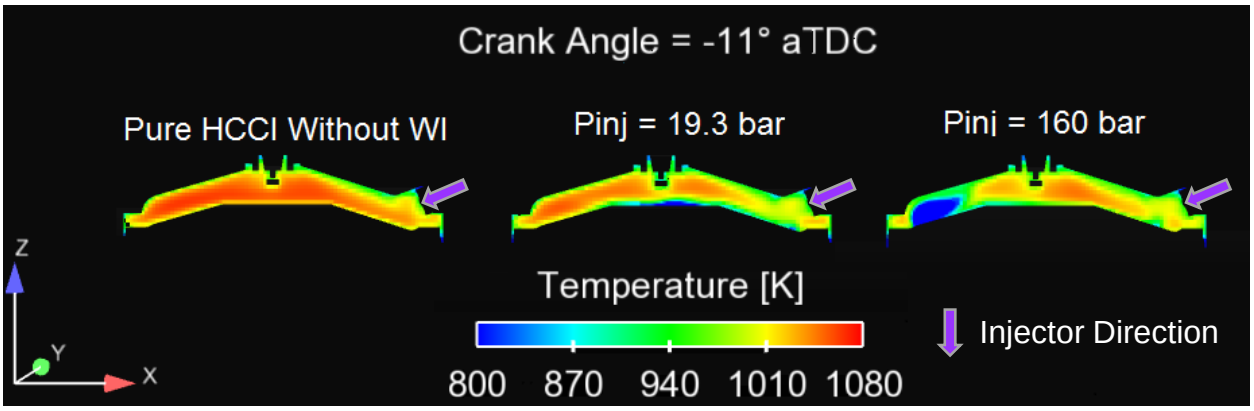

Figure 6. Effect of water injection pressure on cut-plane temperature distribution

Figure 6 shows a 2D cut-plane diagram of the temperature distribution in the cylinder at -11° CAD aTDC for the three cases shown in Figure 5. As shown in Figure 6, increasing the injection pressure results in lower temperatures overall, but also results in a less homogenous temperature distribution and increased thermal stratification.

The thermal width, which is another metric for quantifying the level of thermal stratification, is shown in Figure 7 for the different injection pressures. The thermal width is defined as the temperature distance between the 10% and 90% locations (or 25% and 75%, respectively) on the mass-temperature distribution. As demonstrated in Figure 7, WI at 19.3 bar increases the 10%-90% and 25%-75% thermal width by 54% and 35% at -10° CAD, respectively, compared to the pure HCCI case. Moreover, increasing the injection pressure increases the thermal widths further. Interestingly, the 10%-90% thermal widths for the 19.3 bar injection pressure case increase at a constant rate from SOI to -10 CAD aTDC, when the heat release process begins; however, the higher injection pressures increase at a much faster rate, and reach an inflection point between -25 and -20 CAD aTDC. The reason for this discrepancy is that at lower injection pressures, the breakup and evaporation processes happen more slowly, causing a shallower slope of the thermal width curve versus crank angle. At higher injection pressures, the breakup and evaporation processes happen much more quickly, causing the steeper slope of the thermal widths at higher injection pressures.

There is an analytical post-processing technique called the Thermal Stratification Analysis (TSA) which can determine a mass-temperature distribution and thermal width from the experimental data and heat release characteristics (see [21, 53-56] for more details on the analytical post-processing technique). The 25%-75% thermal width for the pure HCCI case and the 19.3 injection pressure from the experimental and the TSA technique were 56 K and 67 K [21] which agree very well with the values at -10 CAD from the CFD of 53 K and 69 K. The good agreement between the CFD and the experimental thermal widths provides confidence in the accuracy of the results and the analysis.

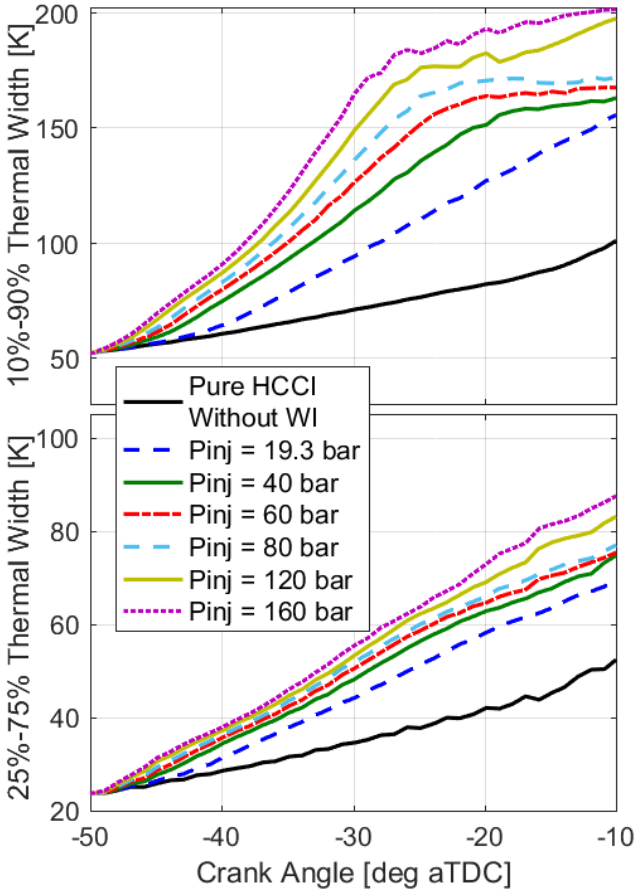

Figure 7. Thermal widths as a function of crank angle for different injection pressures

Figure 8 shows the amount of gaseous water due to evaporation for the various injection pressures as a fraction of the total injected water. As the injection pressure increases, the water droplets evaporate more quickly. This figure proves that increasing the injection pressure results in faster breakup and evaporation of the droplets, which helps explain the trends seen in the thermal widths in Figure 7.

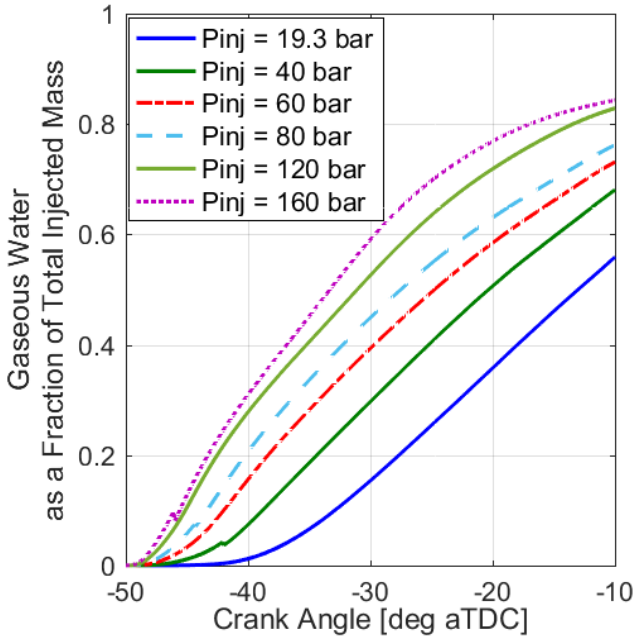

Figure 8. The effect of injection pressure on the fraction of gaseous water versus CAD

As indicated in Figure 4, water injection decreases the heat release rate and delays the start of combustion. The following study was performed to decouple the effects of water injection and combustion phasing to better understand the effects of water injection alone on the rate of heat release. To achieve this goal, the initial temperatures at IVO in the case of pure HCCI without water injection and TSCI with water injection with P_{inj} = 160 bar were adjusted to match the CA50 to the TSCI case with water injection at P_{inj} = 19.3 bar. The mass of injected water was 6.7 mg for both P_{inj} = 19.3 bar and P_{inj} = 160 bar. Figure 9 shows the pressures, heat release rates, and mass fraction burned curves for the three aforementioned cases with matched CA50. Figure 9 indicates that water injection reduces the peak HRR and peak pressure even when CA50 is kept constant. Water injection at a pressure of 19.3 bar decreases peak HRR and peak pressure by 43% and 10%, respectively, compared to the pure HCCI case when the same combustion phasing is considered. Increasing the injection pressure to 160 bar results in a further reduction of the peak HRR and peak pressure (57% and 16%). Also shown in Figure 9 is the mass fraction burned curves which show that WI results in longer 10%-90% burn duration, even when the CA50 combustion phasing is constant.

Effect of Spray Pattern on Combustion

The water spray characteristics are analyzed in more detail in this section, including varying the number of nozzle holes and the arrangement of the nozzle holes (Figure 10). Details of the injection event are listed in Table 4. Within the same number of nozzle holes, all of the injection parameters were kept constant. However, when the number of holes changed (for example, from 6 to 4 to 3 to 2 and finally to 1), the discharge coefficient was adjusted such that the mass, duration, and pressure of injection were constant for all cases.

TABLE 4. INJECTION SPECIFICATIONS

SOI	-50° CAD
Injected water mass	2.5 mg
Injected water pressure	80 bar

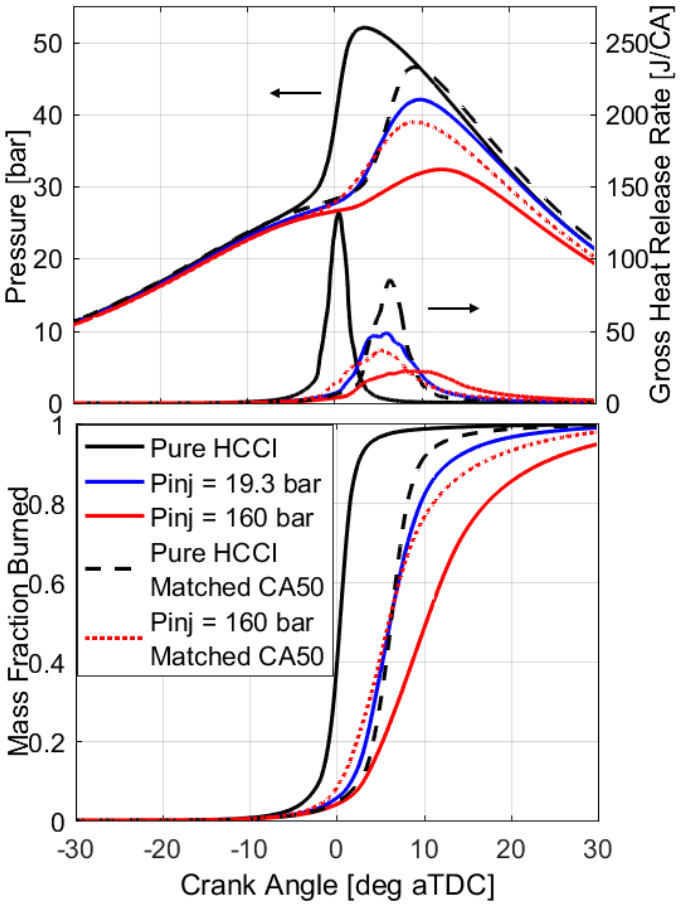

Figure 9. The effect of water injection pressure on the a) cylinder pressure and heat release rates and b) mass fraction burned for pure HCCI and TSCI with matched CA50s

Effect of the number of nozzle holes on combustion: In this section, injectors with 1 through 6 nozzle holes are compared to understand the effect of the number of nozzle holes on thermal stratification and combustion. For the 2-, 3-, and 4-hole injector, one representative pattern of each is shown to simplify the comparison. The difference between the patterns are considered in more detail in the subsequent subsections.

Figure 11 shows the heat release rates for the nozzle hole number comparison. Increasing the number of nozzle holes from 1 to 4 decreased the peak heat release rate due to a better distribution of water throughout the combustion chamber. Further increasing the number of nozzle holes to 6 did not

significantly affect the heat release rate profiles. The reductions of peak heat release rate for 1, 2, 3, 4, and 6 nozzle holes are 36.8%, 39.2%, 46.1%, 50%, and 47.6%, respectively, compared to pure HCCI.

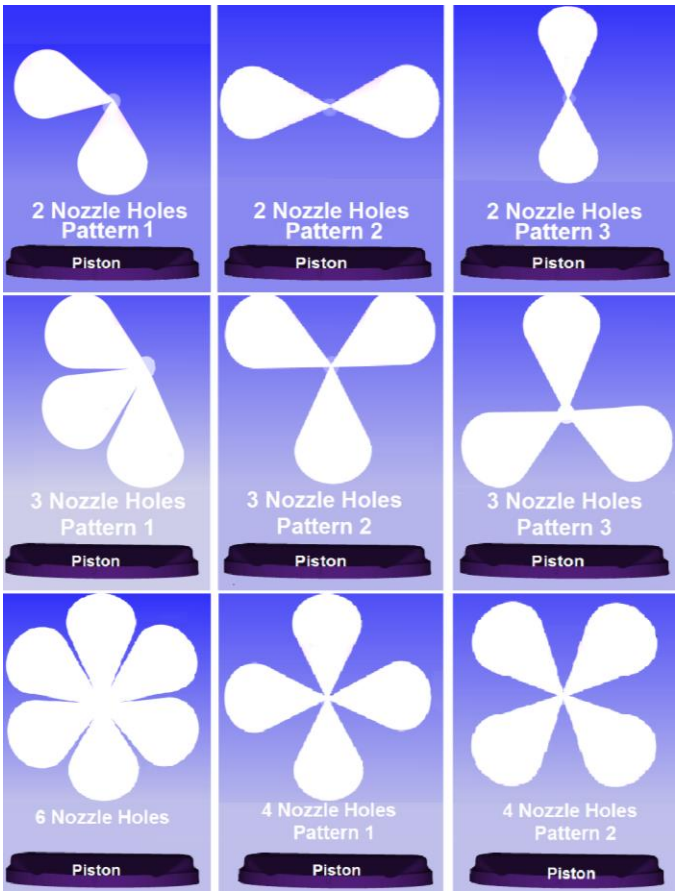

Figure 10. Schematic of spray patterns viewed from a plane perpendicular to injector axis

Figure 12 shows the fraction of total injected water that is trapped in the wall film (i.e. the layer of liquid water adhered to the wall) as a fraction of the total injected mass for the different number of nozzle holes. Increasing the number of nozzle holes reduces the mass of water trapped in the wall film due to better breakup and evaporation and decreased spray penetration. With a higher fraction of mass in the wall film, there is a smaller fraction of water that contributes to increasing thermal stratification. The wall film mass for the 1-hole and 2-hole injectors at TDC is 21% and 13% of the total injected mass respectively.

Overall, increasing the number of nozzle holes broadened the temperature distribution and increased the thermal stratification. This effect is most significant when the number of nozzle holes increases from 1 to 2 to 3, with only small differences between the cases with 3, 4, and 6 nozzle holes. The 10%-90% and 25%-75% thermal widths are shown for the comparison of the number of nozzle holes in Figure 13. Both thermal widths increased with the number of nozzle holes. This increase was more prevalent before -20° CAD aTDC for the 10%-90% thermal width and before -17° CAD aTDC for the 25%-75% thermal width, but dissipated closer to TDC.

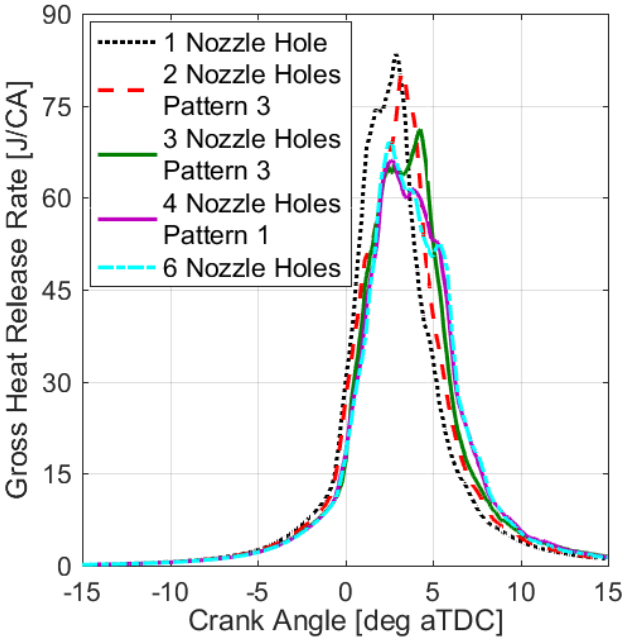

Figure 11. Effect of the number of nozzle holes on the heat release rates

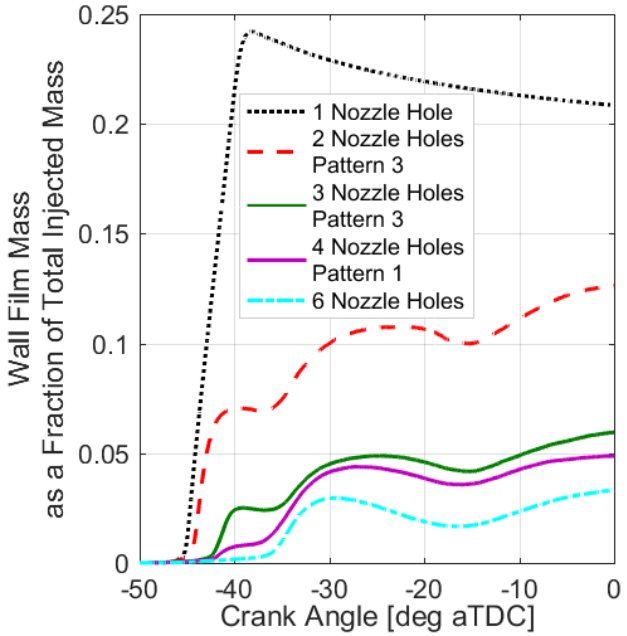

Figure 12. Fraction of injected water trapped in the wall film for the nozzle hole number comparison

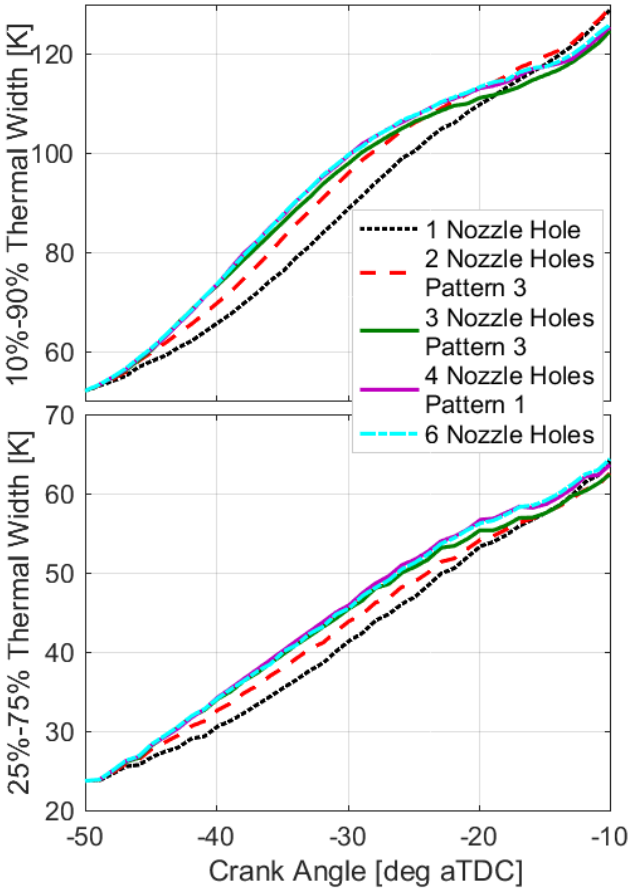

Figure 13. Thermal widths for the nozzle hole number comparison

6-hole and 4-hole Pattern Comparison: An injector with 6 nozzle holes and two different injectors with 4 nozzle holes were investigated as shown in Figure 10. The only difference between Patterns 1 and 2 of the 4-hole injectors is the location of the nozzle holes where Pattern 2 is rotated 45° in the plane perpendicular to nozzle axis compared to Pattern 1.

The heat release rates for the three different spray patterns are shown in Figure 14. According to this figure, the heat release rates for these three different patterns are very similar. The peak heat release rate reduced using the 6-hole, 4-hole Pattern 1, and 4-hole Pattern 2 by 48%, 50%, and 47% respectively compared to pure HCCI without water injection. The 4-hole Pattern 2 has the highest peak heat release rate, and has the narrowest width of the heat release, although the differences are very subtle. It was thus concluded that for injectors with larger number of nozzle holes, the effect of water injection on ignition and heat release rate of TSCI does not depend on the arrangement of the nozzle holes.

Figure 15 shows the mass PDF for the three spray patterns in the last row of Figure 10. According to Figure 15, the mass-temperature distribution has almost the same width in all 3 different patterns. The strong peak that exists in the 4-hole Pattern 2 is not as severe in the 6-hole pattern or the 4-hole Pattern 1. Additionally, the width of the mass-temperature distribution for the 4-hole Pattern 2 is slightly narrower than the other two patterns, which is consistent with the subtle differences seen in the heat release rates.

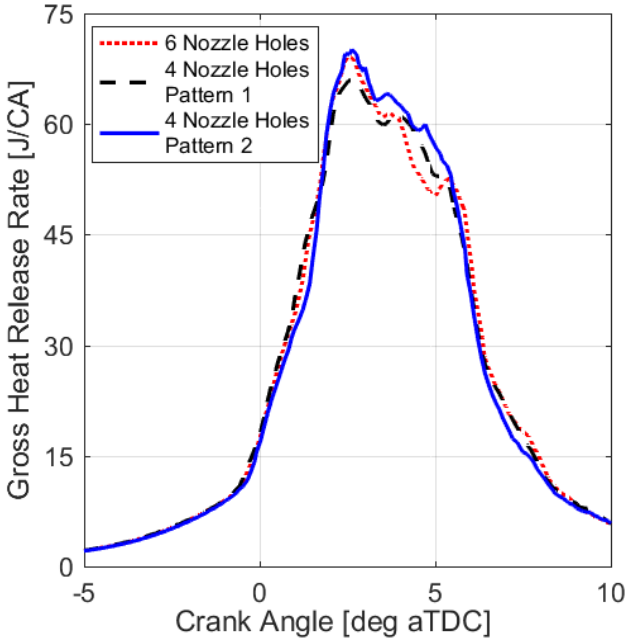

Figure 14. Effect of water injection spray pattern on heat release rate in the 4-hole and 6-hole injectors

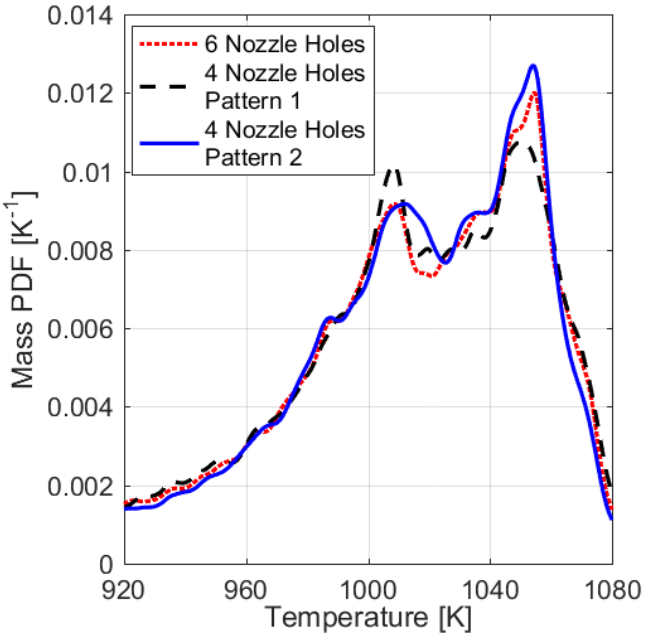

Figure 15. Effect of water injection spray pattern on the mass-temperature distribution prior to ignition for the 4-hole and 6-hole injectors

3-hole Pattern Comparison: Injectors with 3 nozzle holes were simulated using three different spray patterns, including one non-symmetric (Pattern 1) and two symmetric (Patterns 2 and 3). The

second row of Figure 10 shows a schematic of these three patterns.

Figure 16 shows the effect of the three spray patterns described above on the heat release rate. Pattern 3 reduces the peak heat release rate further than Patterns 1 and 2. It is also noticeable that the difference between the peak heat release rates of the non-symmetric Pattern 1 and symmetric Pattern 2 is very small (Pattern 2 is only slightly more effective at decreasing the peak heat release rates), while the difference between the two symmetric patterns is more significant. The peak heat release rate is reduced by 39.9%, 41.33%, and 46.1% using spray Patterns 1, 2, and 3, respectively, compared to pure HCCI without water injection.

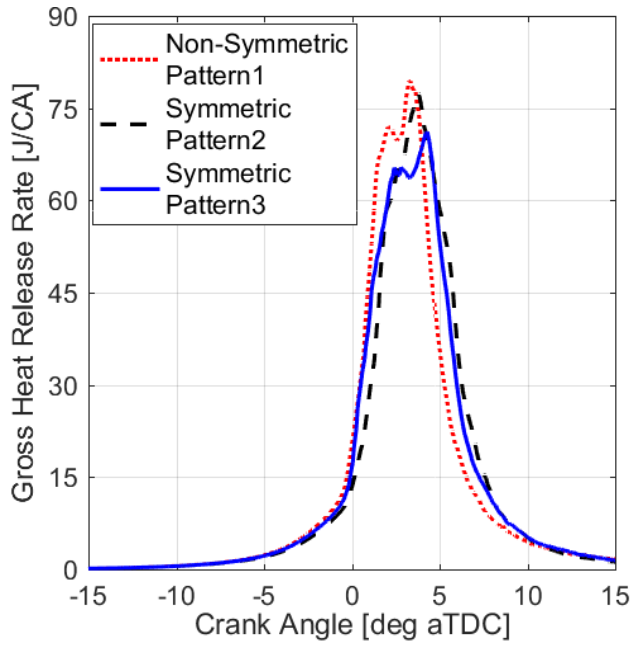

Figure 16. Effect of water injection spray pattern on combustion for the three nozzle hole injectors

Figure 17 shows the mass-temperature distribution for the three different 3-hole injectors at -11 CAD aTDC. As can be seen in Figure 17, the mass-temperature distribution resulting from Pattern 3 is the broadest with the lowest peak in the distribution. This feature of the mass-temperature distribution is responsible for the lower peak heat release rate shown in Figure 16.

2-hole Pattern Comparison: The effect of water injection on ignition and heat release was also simulated for three different spray patterns using a 2-hole injector including one non-symmetric (Pattern 1) and two symmetric (Patterns 2 and 3).

Figure 18 shows the heat release rate for the three different spray patterns described in the first row of Figure 10, and indicates very small effect of the spray pattern on ignition and heat release when a 2-hole injector is used. Pattern 2 is slightly more effective at reducing the peak, while Pattern 3 appears to be slightly more successful at broadening the width of the heat release rate. The mass-temperature distributions shown in Figure 19 exhibit only small differences but Pattern 3 has a somewhat broader mass-temperature distribution than Patterns 1 and 2, which explains its marginally longer heat release duration.

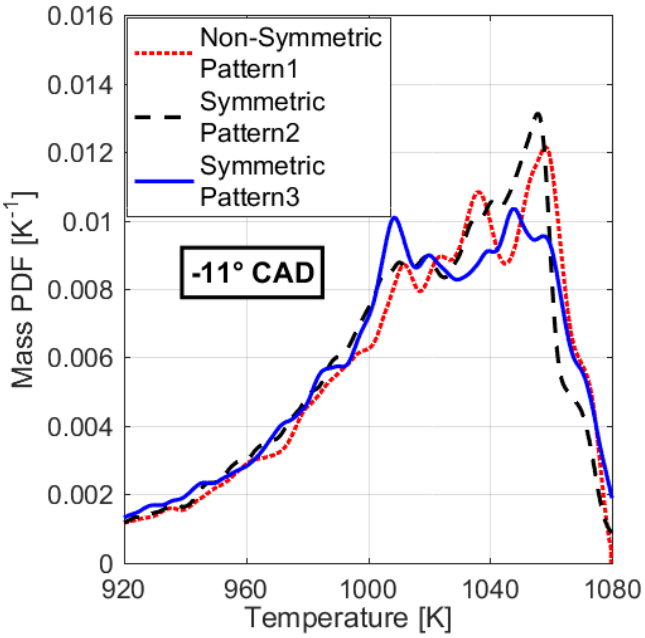

Figure 17. Effect of water injection spray pattern on maas-temperature distribution for the 3-hole injector comparison

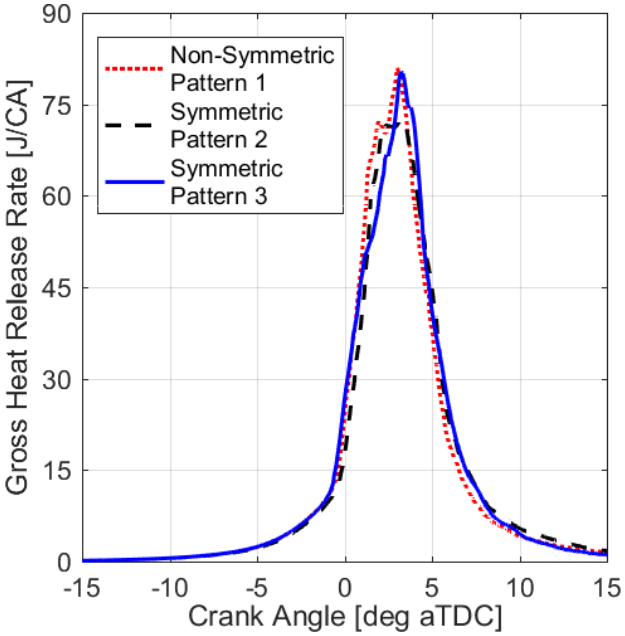

Figure 18. Effect of water injection spray pattern on heat release for the 2-hole injector comparison

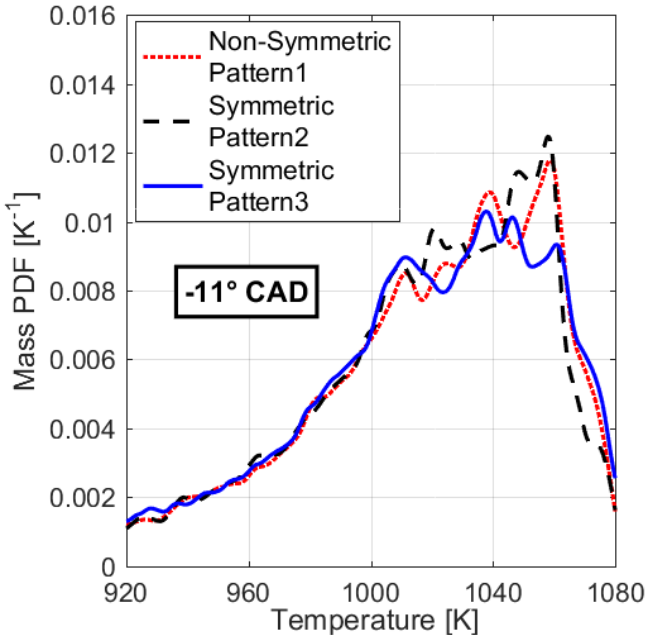

Figure 19. Effect of water injection spray pattern on mass-temperature distribution for the 2-hole injector comparison

CONCLUSIONS

A 3D CFD model of a low temperature combustion HCCI engine was developed to investigate the effect of water injection on combustion, utilizing a new advanced combustion concept called Thermally Stratified Compression Ignition (TSCI). The CFD model was validated against experimental data for both pure HCCI without water injection and TSCI with water injection. The following conclusions can be drawn:

1. Direct injecting water into the combustion chamber increases the level of thermal stratification prior to ignition and provides a means to control the start and rate of combustion in LTC.
2. Increasing the water injection pressure amplifies the effects of water injection, further delaying the start of combustion and reducing the peak pressure and heat release rate.
3. The reduced heat release rates and cylinder pressures as the water injection pressure increased were attributed to a significantly broader mass-temperature distribution, which stemmed from better breakup and increased evaporation rates at higher injection pressures.
4. Increasing the number of injector nozzle holes from 1 to 4 results in a broader mass-temperature distribution and increases the thermal stratification due to a reduced portion of injected water adhered to the wall, as well as better breakup and evaporation.
5. For an injector with the same number of nozzle holes, the spray pattern only slightly affects the level of thermal stratification, where symmetric patterns exhibited faster breakup and evaporation.

TSCI is a new low temperature combustion concept that offers the ability to control both the start and rate of combustion on a cycle-by-cycle basis without any risk of soot or NOx emissions. These results and conclusions help to better understand the spray characteristics and their effects on the temperature distribution and heat release process in TSCI.

ACRONYMS

aTDC – after Top Dead Center
BMEP – Brake Mean Effective Pressure
CA10-90 – Burn duration
CA50 – Crank Angle of 50% burned location
CAD – Crank Angle Degrees
CFR – Co-operative Fuel Research
CO – Carbon Monoxide
DI – Direct Injection
EGR – Exhaust Gas Recirculation
EVC – Exhaust Valve Closing
GCI – Gasoline Compression Ignition
GDCI – Gasoline Direct Injection Compression Ignition
GDI– Gasoline Direct Injection
HCCI – Homogeneous Charge Compression Ignition
HRR – Heat Release Rate
IMEP – Indicated Mean Effective Pressure
IVC – Intake Valve Closing
IVO – Intake Valve Opening
LTC – Low Temperature Combustion
NO_x – Oxides of Nitrogen (NO or NO2)
PCCI – Premixed Charge Compression Ignition
PDF – Probability Density Function
PFS – Partial Fuel Stratification
P_{inj} – Injection Pressure
PRF – Primary Reference Fuel
RCCI – Reactivity Controlled Compression Ignition
SI – Spark Ignition
SOI – Start of Injection
TDC – Top Dead Center
TSCI – Thermally Stratified Compression Ignition
UHC – unburned Hydrocarbon
VCR – Variable Compression Ratio
WI – Water Injection

REFERENCES

[1] 2015, "Quadrennial Technology Review 2015," U.S. Department of Energy
[2] Yao, M., Chen, Z., Zheng, Z., Zhang, B., and Xing, Y., 2006, "Study on the controlling strategies of homogeneous charge compression ignition combustion with fuel of dimethyl ether and methanol," Fuel, 85(14), pp. 2046-2056.
[3] Yao, M., Zheng, Z., and Liu, H., 2009, "Progress and recent trends in homogeneous charge compression ignition (HCCI) engines," Progress in Energy and Combustion Science, 35(5), pp. 398-437.
[4] Yao, M., Zhang, B., Zheng, Z., Chen, Z., and Xing, Y., 2007, "Effects of exhaust gas recirculation on combustion and emissions of a homogeneous charge compression ignition engine

fuelled with primary reference fuels," Proceedings of the Institution of Mechanical Engineers, Part D: Journal of Automobile Engineering, 221(2), pp. 197-213.
[5] Yap, D., Wyszynski, M., Megaritis, A., and Xu, H., 2005, "Applying boosting to gasoline HCCI operation with residual gas trapping," No. 0148-7191, SAE Technical Paper.
[6] Cairns, A., and Blaxill, H., 2005, "The effects of combined internal and external exhaust gas recirculation on gasoline controlled auto-ignition," No. 0148-7191, SAE Technical Paper.
[7] Hyvönen, J., Haraldsson, G., and Johansson, B., 2003, "Operating range in a multi cylinder HCCI engine using variable compression ratio," No. 0148-7191, SAE Technical Paper.
[8] Aroonsrisopon, T., Werner, P., Waldman, J. O., Sohm, V., Foster, D. E., Morikawa, T., and Iida, M., 2004, "Expanding the HCCI operation with the charge stratification," No. 0148-7191, SAE Technical Paper.
[9] Berntsson, A. W., and Denbratt, I., 2007, "HCCI combustion using charge stratification for combustion control," No. 0148-7191, SAE Technical Paper.
[10] Aoyama, T., Hattori, Y., Mizuta, J. i., and Sato, Y., 1996, "An experimental study on premixed-charge compression ignition gasoline engine," No. 0148-7191, SAE Technical Paper.
[11] Flynn, P. F., Hunter, G. L., Zur Loye, A. O., Akinyemi, O. C., Durrett, R. P., Moore, G. A., Muntean, G. G., Peters, L. L., Pierz, P. M., and Wagner, J. A., 2001, "Premixed charge compression ignition engine with optimal combustion control," Google Patents.
[12] Tsolakis, A., and Megaritis, A., 2005, "Partially premixed charge compression ignition engine with on-board H2 production by exhaust gas fuel reforming of diesel and biodiesel," International Journal of Hydrogen Energy, 30(7), pp. 731-745.
[13] Kodavasal, J., Kolodziej, C., Ciatti, S., and Som, S., "CFD Simulation of Gasoline Compression Ignition," Proc. ASME 2014 Internal Combustion Engine Division Fall Technical Conference, American Society of Mechanical Engineers, pp. V002T006A008-V002T006A008.
[14] Kodavasal, J., Kolodziej, C. P., Ciatti, S. A., and Som, S., 2015, "Computational fluid dynamics simulation of gasoline compression ignition," Journal of Energy Resources Technology, 137(3), p. 032212.
[15] Kolodziej, C., Kodavasal, J., Ciatti, S., Som, S., Shidore, N., and Delhom, J., 2015, "Achieving stable engine operation of gasoline compression ignition using 87 AKI gasoline down to idle," No. 0148-7191, SAE Technical Paper.
[16] Sellnau, M., Sinnamon, J., Hoyer, K., and Husted, H., 2011, "Gasoline direct injection compression ignition (GDCI)-diesel-like efficiency with low CO2 emissions," SAE International Journal of Engines, 4(2011-01-1386), pp. 2010-2022.
[17] Yang, Y., Dec, J. E., Dronniou, N., Sjöberg, M., and Cannella, W., 2011, "Partial fuel stratification to control HCCI heat release rates: fuel composition and other factors affecting pre-ignition reactions of two-stage ignition fuels," SAE International Journal of Engines, 4(2011-01-1359), pp. 1903-1920.
[18] Kokjohn, S., Hanson, R., Splitter, D., Kaddatz, J., and Reitz, R. D., 2011, "Fuel reactivity controlled compression ignition (RCCI) combustion in light-and heavy-duty engines," SAE International Journal of Engines, 4(2011-01-0357), pp. 360-374.
[19] Kokjohn, S., Hanson, R., Splitter, D., and Reitz, R., 2011, "Fuel reactivity controlled compression ignition (RCCI): a pathway to controlled high-efficiency clean combustion," International Journal of Engine Research, 12(3), pp. 209-226.
[20] Splitter, D., Hanson, R., Kokjohn, S., and Reitz, R. D., 2011, "Reactivity controlled compression ignition (RCCI) heavy-duty engine operation at mid-and high-loads with conventional and alternative fuels," No. 0148-7191, SAE Technical Paper.
[21] Lawler, B., Splitter, D., Szybist, J., and Kaul, B., 2017, "Thermally Stratified Compression Ignition: A new advanced low temperature combustion mode with load flexibility," Applied Energy, 189, pp. 122-132.
[22] Bedford, F., Rutland, C., Dittrich, P., Raab, A., and Wirbeleit, F., 2000, "Effects of direct water injection on DI diesel engine combustion," No. 0148-7191, SAE Technical Paper.
[23] Brusca, S., and Lanzafame, R., 2001, "Evaluation of the effects of water injection in a single cylinder CFR cetane engine," No. 0148-7191, SAE Technical Paper.
[24] Dickey, D. W., Ryan, T. W., and Matheaus, A. C., 1998, "NOx control in heavy-duty diesel engines-what is the limit?," No. 0148-7191, SAE Technical Paper.
[25] Hountalas, D. T., Mavropoulos, G., and Zannis, T., 2007, "Comparative evaluation of EGR, intake water injection and fuel/water emulsion as NOx reduction techniques for heavy duty diesel engines," No. 0148-7191, SAE Technical Paper.
[26] Hountalas, D. T., Mavropoulos, G. C., Zannis, T., and Mamalis, S., 2006, "Use of water emulsion and intake water injection as NOx reduction techniques for heavy duty diesel engines," No. 0148-7191, SAE Technical Paper.
[27] Nishijima, Y., Asaumi, Y., and Aoyagi, Y., 2002, "Impingement spray system with direct water injection for premixed lean diesel combustion control," No. 0148-7191, SAE Technical Paper.
[28] Psota, M., Easley, W., Fort, T., and Mellor, A., 1997, "Water injection effects on NOx emissions for engines utilizing diffusion flame combustion," No. 0148-7191, SAE Technical Paper.
[29] Brusca, S., and Lanzafame, R., 2003, "Water Injection in IC-SI Engines to Control Detonation and to Reduce Pollutant Emissions," No. 0148-7191, SAE Technical Paper.
[30] Nicholls, J., Ei-Messiri, I., and Newhali, H., 1969, "Inlet manifold water injection for control of nitrogen oxides—theory and experiment," No. 0148-7191, SAE Technical Paper.
[31] Christensen, M., and Johansson, B., 1999, "Homogeneous charge compression ignition with water injection," No. 0148-7191, SAE Technical Paper.
[32] Iwashiro, Y., Tsurushima, T., Nishijima, Y., Asaumi, Y., and Aoyagi, Y., 2002, "Fuel consumption improvement and operation range expansion in HCCI by direct water injection," No. 0148-7191, SAE Technical Paper.
[33] Kaneko, N., Ando, H., Ogawa, H., and Miyamoto, N., 2002, "Expansion of the operating range with in-cylinder water

injection in a premixed charge compression ignition engine," No. 0148-7191, SAE Technical Paper.
[34] Steinhilber, T., and Sattelmayer, T., 2006, "The effect of water addition on HCCI diesel combustion," No. 0148-7191, SAE Technical Paper.
[35] Richards, K., Senecal, P., and Pomraning, E., 2014, "Converge (v2. 2.0)," Theory Manual, Convergent Science, Madison, WI.
[36] Liu, Y.-D., Jia, M., Xie, M.-Z., and Pang, B., 2012, "Enhancement on a skeletal kinetic model for primary reference fuel oxidation by using a semidecoupling methodology," Energy & Fuels, 26(12), pp. 7069-7083.
[37] Amsden, A., 1997, "KIVA3V. A Block-Structured KIVA Program for Engines with Vertical or Canted Valves," Los Alamos National Lab., NM (United States).
[38] Han, Z., and Reitz, R. D., 1995, "Turbulence modeling of internal combustion engines using RNG κ-ε models," Combustion science and technology, 106(4-6), pp. 267-295.
[39] Yakhot, V., and Orszag, S. A., 1986, "Renormalization group analysis of turbulence. I. Basic theory," Journal of scientific computing, 1(1), pp. 3-51.
[40] Beale, J. C., and Reitz, R. D., 1999, "Modeling spray atomization with the Kelvin-Helmholtz/Rayleigh-Taylor hybrid model," Atomization and sprays, 9(6).
[41] Reitz, R. D., and Bracco, F., 1986, "Mechanisms of breakup of round liquid jets," Encyclopedia of fluid mechanics, 3, pp. 233-249.
[42] Su, T., Patterson, M., Reitz, R. D., and Farrell, P., 1996, "Experimental and numerical studies of high pressure multiple injection sprays," No. 0148-7191, SAE Technical Paper.
[43] Liu, A. B., Mather, D., and Reitz, R. D., 1993, "Modeling the effects of drop drag and breakup on fuel sprays," DTIC Document.
[44] Schmidt, D. P., and Rutland, C., 2000, "A new droplet collision algorithm," Journal of Computational Physics, 164(1), pp. 62-80.
[45] Chiang, C., Raju, M., and Sirignano, W., 1992, "Numerical analysis of convecting, vaporizing fuel droplet with variable properties," International journal of heat and mass transfer, 35(5), pp. 1307-1324.
[46] Senecal, P., Pomraning, E., Richards, K., Briggs, T., Choi, C., McDavid, R., and Patterson, M., 2003, "Multi-dimensional modeling of direct-injection diesel spray liquid length and flame lift-off length using CFD and parallel detailed chemistry," No. 0148-7191, SAE Technical Paper.
[47] Babajimopoulos, A., Assanis, D., Flowers, D., Aceves, S., and Hessel, R., 2005, "A fully coupled computational fluid dynamics and multi-zone model with detailed chemical kinetics for the simulation of premixed charge compression ignition engines," International journal of engine research, 6(5), pp. 497-512.
[48] Raju, M., Wang, M., Dai, M., Piggott, W., and Flowers, D., 2012, "Acceleration of Detailed Chemical Kinetics Using Multi-Zone Modeling for CFD in Internal Combustion Engine Simulations," No. 0148-7191, SAE Technical Paper.
[49] Amsden, A. A., O'rourke, P., and Butler, T., 1989, "KIVA-II: A computer program for chemically reactive flows with sprays," Los Alamos National Lab., NM (USA).
[50] Arcoumanis, C., Gavaises, M., Argueyrolles, B., and Galzin, F., 1999, "Modeling of pressure-swirl atomizers for GDI engines," No. 0148-7191, SAE Technical Paper.
[51] Bruno, B. A., Santavicca, D. A., and Zello, J. V., 2003, "Fuel injection pressure effects on the cold start performance of a GDI engine," No. 0148-7191, SAE Technical Paper.
[52] Lee, S., and Park, S., 2014, "Experimental study on spray break-up and atomization processes from GDI injector using high injection pressure up to 30MPa," International Journal of Heat and Fluid Flow, 45, pp. 14-22.
[53] Lawler, B., Hoffman, M., Filipi, Z., Güralp, O., and Najt, P., 2012, "Development of a postprocessing methodology for studying thermal stratification in an HCCI engine," Journal of Engineering for Gas Turbines and Power, 134(10), p. 102801.
[54] Lawler, B., Joshi, S., Lacey, J., Guralp, O., Najt, P., and Filipi, Z., "Understanding the effect of wall conditions and engine geometry on thermal stratification and HCCI combustion," Proc. ASME 2014 Internal Combustion Engine Division Fall Technical Conference, American Society of Mechanical Engineers, pp. V001T003A020-V001T003A020.
[55] Lawler, B., Lacey, J., Dronniou, N., Dernotte, J., Dec, J. E., Guralp, O., Najt, P., and Filipi, Z., 2014, "Refinement and Validation of the Thermal Stratification Analysis: A post-processing methodology for determining temperature distributions in an experimental HCCI engine," No. 0148-7191, SAE Technical Paper.
[56] Lawler, B., Mamalis, S., Joshi, S., Lacey, J., Guralp, O., Najt, P., and Filipi, Z., 2017, "Understanding the effect of operating conditions on thermal stratification and heat release in a homogeneous charge compression ignition engine," Applied Thermal Engineering, 112, pp. 392-402.

APPENDIX

Comparison of Filtered and Unfiltered Mass-Temperature Distributions: The figure below shows a comparison between (a) the raw mass-temperature distribution data from CFD and (b) the results of the mass-temperature distribution after using a weak Butterworth filter. This filter was only used for better visualization of the results. As shown in this figure, the difference between the raw and filtered data is very small and the filter that was chosen such that it preserves the peaks in the original data, while providing a smoother appearance that is easier to interpret.

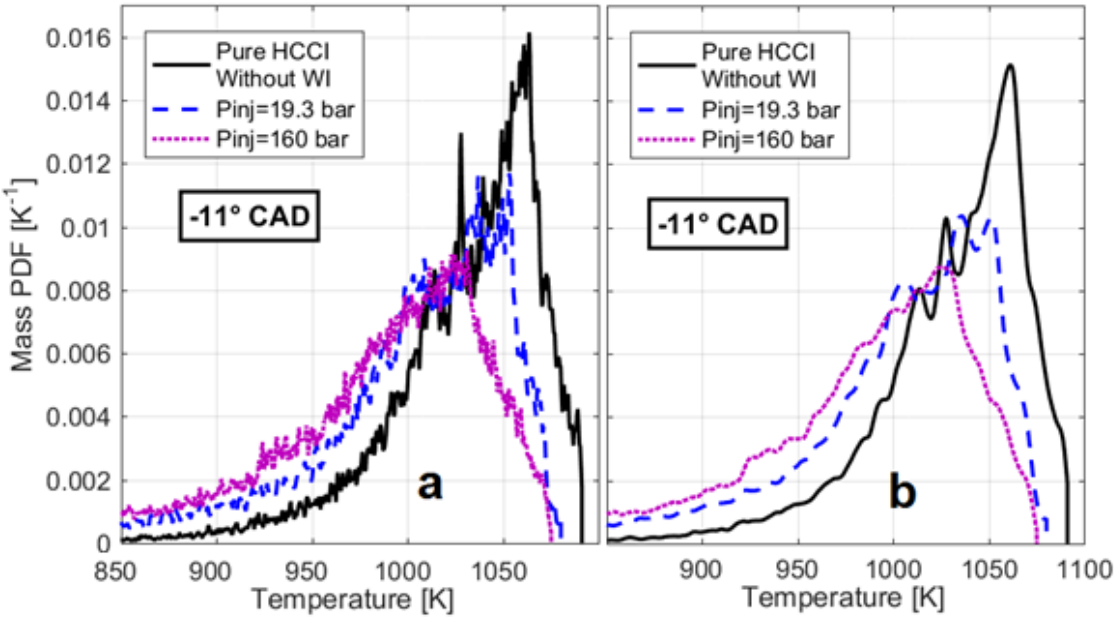

Figure A1. Comparison of filter and unfiltered mass-temperature distribution